ReaxFF Reactive Molecular Dynamics Simulations of Mechano-chemical Decomposition of Perfluoropolyether Lubricants in Heat-assisted Magnetic Recording

Xingyu Chen,† Kento Kawai,‡ Hedong Zhang,,† Kenji Fukuzawa,‡ Nobuaki Koga,† Shintaro Itoh,‡ Naoki Azuma‡*

†Department of Complex Systems Science, Graduate School of Informatics, Nagoya University, Furo-cho, Chikusa-ku, Nagoya 464-8601, Japan

‡Department of Micro-Nano Systems Engineering, Graduate School of Engineering, Nagoya University, Furo-cho, Chikusa-ku, Nagoya 464-8603, Japan

KEYWORDS

Mechano-chemical decomposition, Arrhenius equation, reaction rate, head–disk interface, heat-assisted magnetic recording, perfluoropolyether, molecular dynamics simulation, ReaxFF

ABSTRACT

A thorough understanding of decomposition of perfluoropolyether (PFPE) lubricants is crucial to achieve heat-assisted magnetic recording (HAMR). In contrast to previous studies, which focused on thermal and catalytic decompositions, we gain insights into mechano-chemical decomposition of PFPE films confined between the head and disk by performing reactive molecular dynamics simulations with our new ReaxFF force field. By quantifying the decomposition time constants under the operation conditions of HAMR, we infer that, within the heating time of ~1 ns, pure thermal decomposition hardly occurs, whereas mechano-chemical decomposition is highly likely to occur. The decomposition rate constant of the PFPE films subjected to confined shear increases with normal pressure. The increase is well fitted by a linear stress-activated Arrhenius curve at high normal pressures, whereas this is not the case at low normal pressures. We caution against extrapolating the linear stress-activated Arrhenius curve which could cause significant overestimation of decomposition rate constants at low normal pressures. We find that mechano-chemical decomposition of PFPEs is mainly attributed to the dissociation of C–OH and ether C–O bonds in the polar end groups, and in the main chain the C–O bond is more likely to dissociate than the C–C bond.

1. INTRODUCTION

The emerging era of artificial intelligence and big data stimulates the need for storage of huge amounts of digital information at low cost. Heat-assisted magnetic recording (HAMR) provides one solution to this need because of its potential to largely increase the recording density of hard disk drives by overcoming the tradeoff between writability and thermal stability of magnetic media.[1] In HAMR systems, the magnetic media are heated during the recording process with a laser beam delivered by a near-field transducer (NFT) in the magnetic head. The temperature of the media reaches above the Curie temperature, typically 700–800 K, thereby lowering the coercivity of the media.[2] However, such high operation temperature makes it challenging to ensure the reliability and durability of the head–disk interface (HDI) which is lubricated by perfluoropolyether (PFPE) films coated on disk surfaces at a thickness of 1–2 nm.[3]

One serious concern is decomposition of the PFPE films. As the clearance between the flying head and rotating disk is less than 1 nm and should be reduced preferably to zero to allow for ultra-high recording densities,[4] intermittent contact sliding between the head and disk occurs inevitably, resulting in confined shear of the PFPE films at shear speeds and shear rates up to 50 m/s and 5×10^{10} s^{-1}. The combined impacts of shearing and heating may induce mechano-chemical decomposition of the PFPE films and increase the decomposition rate as compared to pure thermal decomposition. It has been demonstrated that mechano-chemical reactions play a key role in many areas of tribology.[5] In fact, one critical issue in HAMR is accumulation of contaminating materials, which are termed as smears, at the NFT of heads after writing operations.[6] Though the mechanism of smear formation is yet to be fully elucidated, one major factor is transfer of decomposed PFPE fragments from the disk to head.[6–10] Smears may substantially raise the head temperature and affect the media heating process, thereby degrading the long-term reliability and recording performance

of HAMR. Therefore, a thorough understanding of PFPE decomposition under the operation conditions of HAMR is of great significance.

With Fourier transform infrared spectroscopy (FT-IR) or time-of-flight secondary ion mass spectroscopy (TOF-SIMS), the thermal decomposition of PFPEs has been experimentally confirmed to initiate at the polar end groups,[11–13] and the dissociation of main chain occurs when the temperature further increases.[13] It was also confirmed that the main chain dissociation is mainly attributed to the break of C–O–C bond,[11] which is the weakest bond in the main chain of PFPEs.[14,15] Helmick and Jones measured the thermal decomposition temperatures of bulk nonpolar PFPEs and determined the activation energies with the reaction rate theory.[16] Degradation of PFPE films during contact sliding at room temperature was observed using a high-vacuum environmental tribometer equipped with a mass spectrometer and the results suggested that triboelectrical reaction and mechanical scission could be the dominant mechanism for PFPE decomposition.[17–19]

Molecular dynamics (MD) simulations have also been used to study properties of PFPE films.[15,20–26] Particularly, PFPE decomposition has been studied by reactive MD simulations. Compared with density functional theory (DFT) and reactive coarse-grained MD,[24,25] reactive MD with ReaxFF[27–32] force fields is a cost-effective and accurate method providing atomistic-level details of dynamics of systems including chemical reactions, typically more than five orders of magnitude less costly than DFT calculations.[33] Performing ReaxFF MD simulations, Lotfi et al. studied the decomposition of polar PFPE D-4OH at elevated temperatures on diamond-like carbon (DLC) surfaces[15] and in the presence of oxygen, water, and nanoparticles of SiO_2, FeO(OH), and Fe_2O_3.[26] Their simulation results indicated that the PFPE decomposition is accelerated by DLC, water, and the oxide nanoparticles, whereas the effect of oxygen molecules is less significant.

As studies so far mainly focused on thermal and catalytic decompositions of PFPE lubricants, less is known about mechano-chemical decomposition. In addition, decomposition rates of PFPEs, which are particularly critical for HAMR because the time scale of heating process is ~1 ns,[1] are yet to be quantified. Experimental approaches are difficult to access the extreme conditions of high temperature, high shear rate, and short heating time in HAMR. Though high temperature and shear rate are easily achieved in simulations, the heating time is somewhat long for reactive MD simulations. Even with the ReaxFF method, 1-ns simulations are still computationally expensive because a time step as small as ~0.1 fs is typically required for accurate simulation of reaction processes.[15,26] As a compromise, temperatures obviously higher than the actual conditions are usually used to accelerate reactive MD simulations.

In this study, aiming to understand mechano-chemical decomposition of PFPE lubricants in HAMR, we develop the ReaxFF force field of PFPEs, which is not available from the published literature, and conduct ReaxFF reactive nonequilibrium molecular dynamics (NEMD) simulations[34,35] under the operation conditions of HAMR. The time constant of mechano-chemical decomposition is quantified and compared with that of pure thermal decomposition. Although high temperatures are used to accelerate the simulations of pure thermal decomposition, we are able to derive the time constants at the heating temperatures in HAMR by analyzing the simulation results with the reaction rate theory.[29,30,36–38] We also examine the mechano-chemical decomposition pathway of PEPF films and the change in decomposition rate with normal pressure and molecular structure. Specifically, the stress-assisted reaction rate theory[39–42] is applied to analyze the effect of mechanical stress.

2. SIMULATION METHOD AND DETAILS

2.1. ReaxFF Reactive Force Field Method. ReaxFF is a reactive force field method based on bond order,[27,28] which dictates connectivities of atoms and is calculated from the interatomic distances of all pairs of atoms. Updating the bond order at each time step allows for description of bond breaking and bond forming during MD simulations. In ReaxFF the total energy of a system, E_{system}, is described as[29]

$$E_{\mathrm{system}} = E_{\mathrm{bond}} + E_{\mathrm{over}} + E_{\mathrm{under}} + E_{\mathrm{tor}} + E_{\mathrm{val}} + E_{\mathrm{lp}} + E_{\mathrm{vdw}} + E_{\mathrm{coulomb}} \quad (1)$$

where E_{bond}, E_{over}, E_{under}, E_{tor}, E_{val}, E_{lp}, E_{vdw}, E_{coulomb} represent bond energy, overcoordination energy penalty, undercoordination stability, torsion angle energy, valence angle energy, lone pair energy, van der Waals energy, and Coulomb energy, respectively.

In contrast to force fields for nonreactive MD, which are basically general-purpose, ReaxFF force field parameters are usually optimized to reproduce reactions of molecules of interest and thus specific to target molecules.[31,43] After reviewing the published ReaxFF force fields, we confirmed that the ReaxFF force field for Teflon and molecules composed of C, H, and O atoms include most of the parameters for the ReaxFF of PFPE, but parameters for C–O and C–F bonds and O–C–F valence angle need to be added or refined.[44] Therefore, with quantum mechanical (QM) calculations, we first prepared training data regarding (1) change of potential energies with C–O and C–F bond lengths and O–C–F valence angle, (2) dissociation energies of C–O and C–F bonds, (3) optimized structures and the corresponding energies of PFPEs, and (4) energies of various structural isomers of PFPEs. Chemical formulas of the PFPEs will be described in Section 2.2. Then the optimal force field parameters for the training datasets, which ensure the error defined below[29] within desired level, were obtained using the covariance matrix adaptation evolution strategy.

$$\mathrm{Error} = \sum_{i=1}^{n} \left[\frac{X_{i,\mathrm{TS}} - X_{i,\mathrm{ReaxFF}}}{\sigma_i}\right]^2 \quad (2)$$

where n is the total number of the entries of the training sets, $X_{i,\mathrm{TS}}$ and $X_{i,\mathrm{ReaxFF}}$ are the ith training set and the corresponding ReaxFF value, and σ_i is the weighting factor.

The QM calculations were carried out with the Gaussian 16 package[45] using DFT with the B3LYP hybrid functional[46,47] and the 6-31G(d) basis set.[48–50] AMS (Amsterdam Modeling Suite) software,[51] which uses a successive one-parameter parabolic extrapolation approach for the parameterization, was used to find the best fit ReaxFF. We performed five individual optimization runs and calculated the error of each run with Eq. (2). The force field with the lowest error was used in our reactive MD simulations. As will be presented in Section 3.1, the developed ReaxFF force field provides a good representation of the QM calculation results.

2.2. Simulation Models and Procedures. In our reactive MD simulations, we used four types of PFPE lubricants: polar D-4OH and nonpolar Demnum of the Demnum type and polar Z-tetraol and nonpolar Z of the Fomblin type. Their chemical formulas and molecular weights are listed in Table 1. Note that, for the ReaxFF parameterization, only D-4OH and Z-tetraol were used and the number of repeat units in the main chain was set to one to reduce the computational cost of expensive DFT calculations.

To focus on the effect of mechanical stress rather than surface catalyst, as a simplified model of the DLC overcoats on the head and disk surfaces in HAMR, we built diamond crystal plates with (001) surface orientation, which feature high thermal stability.[52] To ensure that the applied shear stress transfers into the lubricant films and to be representative of amorphous surfaces where slip is not expected,[53] slip at the liquid–solid interfaces during shear was suppressed by surface roughness generated on the solid surfaces by removing some carbon atoms and passivating dangling bonds with hydrogen atoms (Figure S1, Supporting Information).[54–56] These surfaces are similar to hydrogenated tetrahedral amorphous carbon (ta-C:H). To effectively suppress slip and

be close to the typical value (0.2 nm) of the arithmetic mean roughness of the head and disk surfaces,[57] the peak-to-valley height and period of the surface roughness were set to 0.27 and 1.0 nm in this study.

Table 1. Chemical formulas and molecular weights of PFPE lubricants.

Lubricant		Chemical formula	Molecular weight (g/mol)
Polar	D-4OH	$X–O–(CF_2CF_2CF_2O)_9–X$	1820
		$X = CF_2CH_2OCH_2CH(OH)CH_2OH$	
	Z-tetraol	$X–O–(CF_2CF_2O)_8–(CF_2O)_8–X$	1782
		$X = CF_2CH_2OCH_2CH(OH)CH_2OH$	
Nonpolar	Demnum	$X–O–(CF_2CF_2CF_2O)_9–X$	1848
		$X = CF_2CF_2CF_3$	
	Z	$X–O–(CF_2CF_2O)_9–(CF_2O)_9–X$	1792
		$X = CF_3$	

To separate the effects of temperature, normal pressure, and shear force on lubricant decomposition, we carried out three types of reactive MD simulations and monitored the progress of decomposition with time. One is for bulk PFPE subjected to heating, the second is for PFPE films coated on the disk subjected to heating and impacting from the head under a constant normal pressure, and the third is for PFPE films coated on the disk subjected to heating and shearing by the head under a constant normal pressure and shear speed. These are simply referred to as heating, impacting, and shearing simulations, respectively. Only D-4OH, which is actually used in hard disk drives, was used for the heating and impacting simulations, and all of the four types of PFPEs were used for the shearing simulation. As will be described in Sections 2.2.1 and 2.2.2, the

temperature was higher and the pressure was lower in the heating simulation than in the impacting and shearing simulations. These led to more rapid atomic motion in the heating simulations, hence the time step was set to 0.1 fs for the heating simulations and 0.2 fs for the impacting and shearing simulations. It should be noted that, to save computational time, initial configurations for the reactive MD simulations were equilibrated by nonreactive MD simulations employing the COMPASS (condensed-phase optimized molecular potentials for atomistic simulation studies) II force field.[58] We confirmed, for the heating simulation at 2500 K, that the results obtained from the initial configurations equilibrated with the COMPASS and developed ReaxFF are consistent within the error margin (Figure S2, Supporting Information). All of the MD simulations in this study were conducted using LAMMPS (Large-scale Atomic/Molecular Massively Parallel Simulator).[59] Other details of the three types of reactive MD simulations are described below.

2.2.1. Heating Simulation. The initial configurations of the heating simulations consisted of 36 D-4OH molecules inside a cubic box with periodic boundaries in the *x*, *y*, and *z* directions, as shown in Figure 1. The system was heated to a target temperature in 4 ps and then fixed at the temperature for 100 ps. To accelerate lubrication decomposition and thus reduce the computational time, the target temperature was set from 2000 to 2500 K with an interval of 100 K, much higher than expected in HAMR. The pressure of the system was fixed at 0.1 MPa. The Nose-Hoover thermostat and barostat were used for the temperature and pressure control.[60,61] To reduce statistical uncertainty, for each temperature, simulations were run with 10 different initial configurations and the results were averaged.

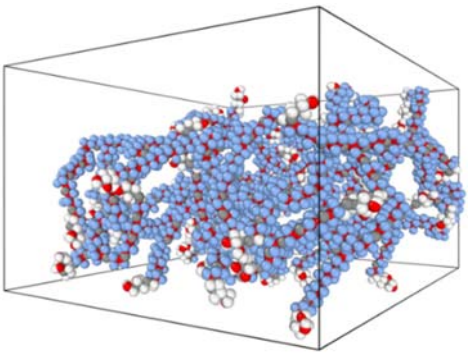

Figure 1. One initial configuration of the heating simulations. The system consisted of 36 D-4OH molecules. The gray, white, blue, and red represent carbon, hydrogen, fluorine, and oxygen atoms, respectively.

2.2.2. Impacting and Shearing Simulations. The initial configurations of the impacting and shearing simulations were similar and one is shown in Figure 2. Lubricant films consisting of 40 PFPE molecules were deposited on the disk located at the bottom of a simulation box, which had dimensions of 8.04624 nm and periodic boundaries in the *x* and *y* directions, and the head was set above the PFPE films. The film thickness, which was defined as the distance between the mean surfaces of the disk and PFPE film, was 1.34 nm. The distance between the mean surfaces of the head and disk was set to 1.70 nm in the impacting simulation so that the head did not contact with the PFPE films initially. In the shearing simulations, to exclude the decomposition induced by collision of the head with the PFPE films as in the impacting simulation, the head–disk distance was set to 1.55 nm so that the head contacted with the PFPE films initially.

Both in the impacting and shearing reactive MD simulations, the systems were heated to a target temperature in 4 ps and then fixed at the temperature. To ensure temperature rise in the PFPE films, the Nose-Hoover thermostat was coupled to the head, films, and disk in the initial 4 ps. After that, the thermostat was removed from the films and interfacial layers (consisting of hydrogen atoms and their bonded carbon atoms) of the head and disk to avoid its unphysical influence on the

dynamics of the films.[62] A constant normal pressure was applied to the head by applying a constant force in the −*z* direction to the carbon atoms in the upmost layer of the head throughout the simulations. In the shearing simulations, in addition to the constant normal pressure, a constant shear speed of 50 m/s in the *x* direction was applied to the head from 4 ps to the end of simulations. To reproduce the operation conditions in HAMR, we set the target temperature and normal pressure to 700 K and 0.1 GPa. At the relatively low temperature and normal pressure, PFPE molecules decomposed slowly and therefore we performed the impacting and shearing simulations for a long time of 1 ns. Constrained by the extremely high computational cost, each simulation was run only one time. To examine the effect of normal pressure on mechano-chemical decomposition, we also varied the normal pressure from 0.5 to 9.8 GPa in the shearing simulations. For each of these relatively high normal pressures, simulations were run with 10 different initial configurations for 200 ps and the results were averaged to reduce statistical uncertainty.

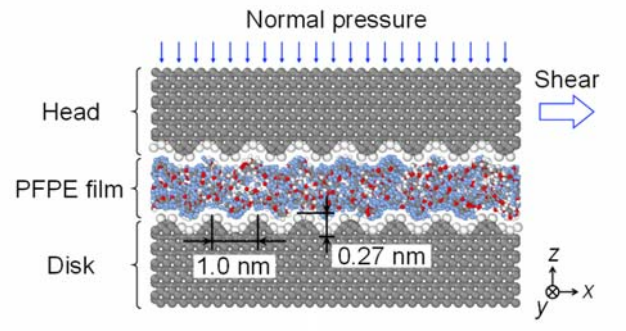

Figure 2. One initial configuration of the shearing simulations. Surface roughness with a peak-to-valley height of 0.27 nm and a period of 1.0 nm was introduced to suppress interfacial slip. The *x* and *y* dimensions of the simulation box were both set to 8.04624 nm, and periodic boundary conditions were applied in the two directions. The gray, white, blue, and red represent carbon, hydrogen, fluorine, and oxygen atoms, respectively.

3. RESULTS AND DISCUSSION

3.1. Validation of PFPE ReaxFF. Figure 3 compares the energies of C–O and C–F bonds and O–C–F valence angle calculated by QM and our developed PFPE ReaxFF. Good agreement is obtained, particularly for the bond dissociation energies and energies in the vicinity of equilibrium. The deviation between the ReaxFF and QM is 1.8 and 0.65 kcal/mol for C–O and C–F bond dissociation energies. The deviation between the ReaxFF and QM averaged over seven data points in the vicinity of equilibrium is 1.3, 2.3, and 0.45 kcal/mol for energies of C–O bond, C–F bond, and O–C–F valence angle. Moreover, the bulk density of D-4OH calculated with the developed ReaxFF at 293 K and 0.1 MPa is 1.76 g/cm^3 (Figure S3, Supporting Information), favorably comparable to the value of 1.7 g/cm^3 provided by the manufacturer of D-4OH. These results demonstrate that the developed ReaxFF force field is reasonably accurate for reactive MD simulations of PFPEs.

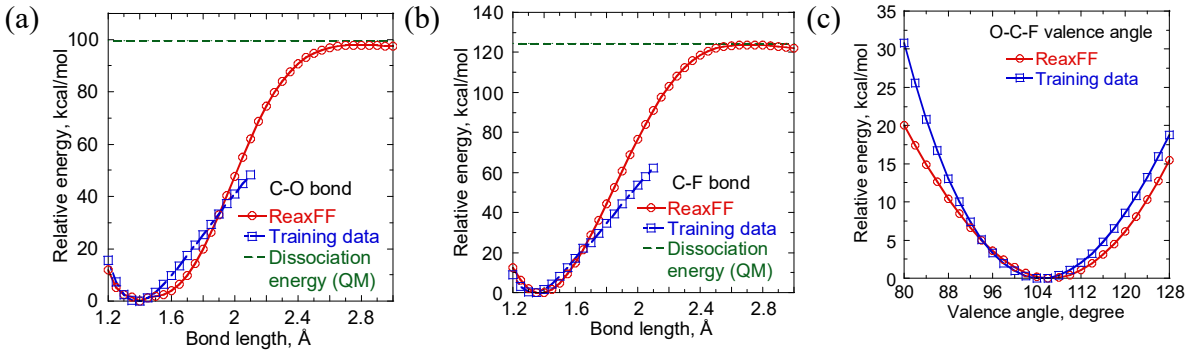

Figure 3. Comparison between results of the developed PFPE ReaxFF and training data from QM calculation: (a) C–O bond energy, (b) C–F bond energy, and (c) O–C–F valence angle energy. The bond dissociation energies (broken lines) in (a) and (b) were obtained by QM calculation.

3.2. Comparison of Time Constants of Pure Thermal and Mechano-chemical Decompositions. Because the heating time in HAMR is in the order of 1 ns, decomposition time constants are a critical criterion for lubricant selection and design. Hence, we compared the time

constants of pure thermal and mechano-chemical decompositions of D-4OH under the operation conditions of HAMR by analyzing the results of the heating, impacting, and shearing simulations.

3.2.1. Pure Thermal Decomposition. To quantify the time constants of pure thermal decomposition of PFPE at arbitrary temperatures, we analyzed the results of the heating simulations using the Arrhenius model. First, we derived the decomposition rate constant k at each temperature by recording the number of intact PFPE molecules as a function of time, N_t, and fitting it with[30]

$$\ln(N_t/N_0) = -kt \tag{3}$$

where t is time and N_0 is the number of intact PFPE molecules at $t = 0$. It should be noted that the first-order kinetics is assumed in Eq. (3), which is reasonable for thermal decomposition of covalent compounds.[29,30,37,63] Then we fitted the reaction decomposition rate constants k at different temperatures T with the Arrhenius equation[30,64]

$$\ln k = \ln A - \frac{E_\mathrm{a}}{k_\mathrm{B}T} \tag{4}$$

where A is a pre-exponential factor, E_a is the activation energy, and k_B is the Boltzmann constant. As a result, we are able to determine the values of A and E_a from the intercept and slope of the fitted line and extrapolate the fitted line to derive decomposition rate constants k at any temperatures of interest. The reciprocal of k is defined as the decomposition time constant.

Figure 4a shows $\ln(N_t/N_0)$ derived from the heating simulations of D-4OH at different temperatures as a function of time. For each temperature, the number of intact D-4OH molecules N_t was averaged over 10 independent simulations. The straight lines are fits to Eq. (3) and the coefficients of determination R^2 are larger than 0.94. This confirms that the thermal decomposition of D-4OH molecules follows the first-order kinetics. It is evident that the decomposition rate constant of D-4OH, which is given by the slopes of the fitted lines, increases with increasing

temperature. At temperatures higher than 2200 K, all of the D-4OH molecules decomposed within 100 ps. Figure 4b shows the Arrhenius plot for the thermal decomposition rates k of D-4OH at different temperatures. The activation energy E_a and pre-exponential factor A were calculated from the fitted straight line and the results are listed in Table 2. As we did not find experimental values for D-4OH in the literature, experimental values for nonpolar Demnum,[16] which has identical main chain structure as D-4OH, are listed in Table 2 for comparison. The activation energy of D-4OH derived from our simulations is slightly smaller than the experimental values of nonpolar Demnum, which is considered reasonable because, as will be presented in Section 3.3.2, our simulation results show that polar D-4OH decomposes more rapidly than nonpolar Demnum. This comparison confirms the validity of our reactive MD simulations with the developed PFPE ReaxFF.

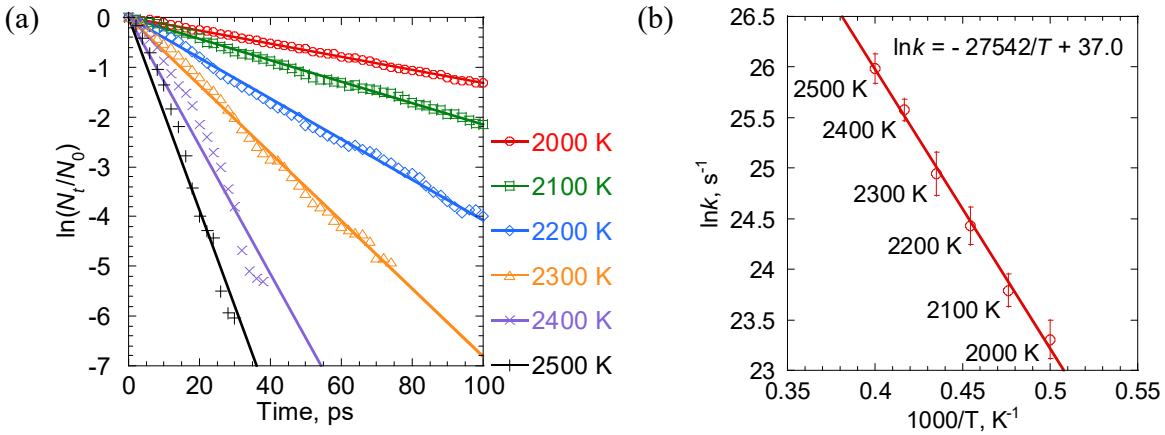

Figure 4. (a) Natural logarithms of ratios between the numbers of intact D-4OH at time t and time zero at different temperatures. For each temperature, the results were averaged over 10 independent heating simulations. The straight lines are fits to Eq. (3). (b) Arrhenius plot for thermal decomposition of D-4OH. The straight line is fit to Eq. (4). The decomposition rate constants k were obtained from the slopes of the fitted lines in (a). Error bar indicates the standard deviation of 10 independent simulations.

Table 2. Comparison of fitted Arrhenius parameters with experimental results.[16]

	E_a (kcal/mol)	A (Hz)
This work	54.7	1.15×10^{16}
Experiment[a]	55.0–63.1	—

[a] Experimental results are for nonpolar Demnum.

By extrapolating the fitted straight line in Figure 4b, we estimated the reaction rate constants k at 700 and 800 K, which are operation temperatures of HAMR, to be 0.094 and 12.854 s^{-1}, respectively. Then, the time constant for pure thermal decomposition of D-4OH was calculated to be 11 and 0.078 s at 700 and 800 K. These time constants are more than seven orders longer than the heating time of approximately 1 ns in HAMR. Consequently, we conclude that pure thermal decomposition hardly occurs within the heating time of HAMR. Nevertheless, we should emphasize that decreasing the temperature from 800 to 700 K leads to an increase of decomposition time constant by approximately two orders and thus a further significantly lowered risk of lubricant decomposition.

3.2.2. Mechano-chemical Decomposition. Figure 5a and b show the time evolution of the number of intact D-4OH during the 1-ns impacting and shearing simulations, respectively. For the impacting simulation, we confirmed that the head crashed into the D-4OH film at the maximum vertical speed of 32 m/s. Despite the relatively low temperature and normal pressure of 700 K and 0.1 GPa, approximately 23 % and 18 % molecules decomposed in the 1-ns impacting and shearing simulations, respectively. By fitting the results with Eq. (3), the decomposition time constants for the impacting and shearing simulations were calculated to 5 and 10 ns, respectively (Figure S4, Supporting Information). Because each type of the simulations was run only one time, we suggest

that the effects of vertical impact and horizontal shear on decomposition time constants are of similar extent. For comparison, the time constants of pure thermal and mechano-chemical decompositions are summarized in Table 3. The time constants of mechano-chemical decomposition are approximately nine orders shorter than that of pure thermal decomposition at 700 K and comparable to the heating time in HAMR. These results indicate the significant influence of mechanical stress on PFPE decomposition. We infer that, under the operation conditions of HAMR, PFPE molecules are highly likely to decompose if subjected to normal impact and/or horizontal shear.

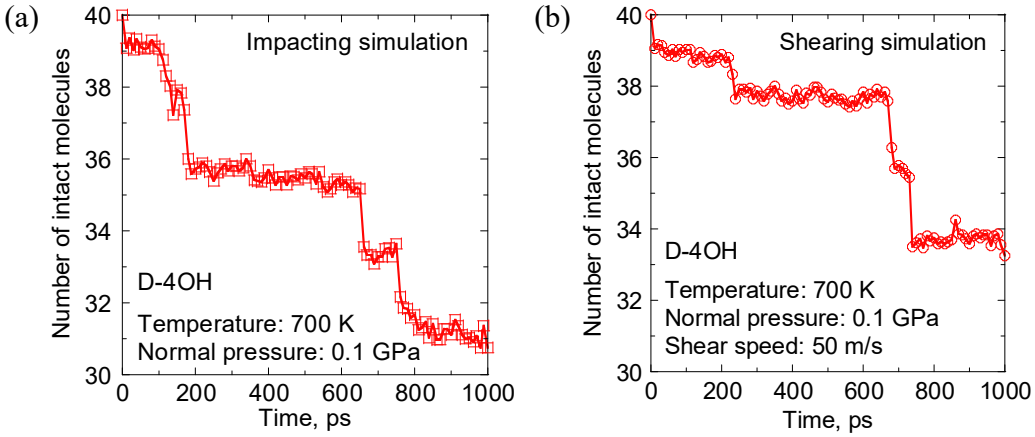

Figure 5. Time evolution of the number of intact D-4OH molecules in the (a) 1-ns impacting simulation and (b) 1-ns shearing simulation.

Table 3. Comparison of time constants of pure thermal and mechano-chemical decompositions.

Conditions	Time constant
Heating (700 K)	11 s
Impacting (700K, 0.1 GPa)	5 ns
Shearing (700 K, 0.1 GPa, 50 m/s)	10 ns

3.3. Characteristics of Mechano-chemical Decomposition. As we confirmed that mechano-chemical decomposition is highly likely to occur rather than pure thermal decomposition in HAMR in the previous section, we will focus on mechano-chemical decomposition of PFPE films and investigate the effects of normal pressure and molecular structure and the reaction pathway in this section. Note that the results presented below were obtained from the shearing simulations, which reflected the realistic situation in HAMR more closely than the impacting simulations.

3.3.1 Effect of Normal Pressure. To study the effect of normal pressure on the mechano-chemical decomposition rate of PFPE films, we varied the normal pressure to 0.5, 1.0, 2.0, 3.9, 5.9, 7.8, and 9.8 GPa in the shearing simulations. The decomposition rate constant at each normal pressure was calculated by fitting the time evolution of the number of intact D-4OH molecules during the 200-ps simulations with Eq. (3) (Figure S5, Supporting Information). The results, together with that of the 1-ns shearing at the normal pressure of 0.1 GPa described in Section 3.2.2, are shown in Figure 6. The decomposition rate constant increases with increasing normal pressure. It is intriguing to note that, at relatively high normal pressures of 3.9–9.8 GPa the change of logarithm of decomposition rate constant with normal pressure can be well fitted by a straight line, whereas data points at 0.1–2.0 GPa lie obviously below the fitted straight line.

To explain these results, we adopt the widely used stress-assisted reaction rate theory, which is extended from the pure thermal Arrhenius theory.[36,39–42] The stress-dependent reaction rate constant k_σ is given by[40]

$$\ln k_\sigma = \ln A - \frac{E_{a\sigma}}{k_B T} \tag{5}$$

Here, $E_{a\sigma}$ is the activation energy in the presence of mechanical stress and is expanded as[38,40,65,66]

$$E_{a\sigma} = E_a - \sigma \Delta V_a \tag{6}$$

$$\sigma = \sigma_0 + \mu P \tag{7}$$

where E_a is the stress-free activation energy, σ is the shear stress, ΔV_a is the activation volume, P is the external normal pressure, σ_0 is the shear stress at $P = 0$, and μ is a constant and can be assumed to be the same as friction coefficient in the absence of substrate wear.[67] Equation (5) is rewritten by substituting Eqs. (6) and (7) as

$$\ln k_\sigma = \ln A - \frac{E_a}{k_B T} + \frac{\sigma_0 \Delta V_a}{k_B T} + \frac{\mu \Delta V_a}{k_B T} P \quad (8)$$

It should be noted that, in Eqs. (6)–(8), shear stress rather than normal pressure is supposed to be the component reducing the activation energy.

From Eq. (8) and the nonlinear increase of $\ln k_\sigma$ with P in Figure 6, it can be known that $\mu \Delta V_a$ is not a constant at low normal pressures. To gain insights, we first determined the value of friction coefficient μ by calculating shear stresses at different normal pressures from the simulations. The result is shown in Figure 7. Data points are well fitted by Eq. (7) with $\sigma_0 = 0$ and $\mu = 0.18$. Because the slopes of the curve of $\ln k_\sigma$ versus P at different normal pressures are determined by $\frac{\mu \Delta V_a}{k_B T}$ according to Eq. (8), we then calculated the activation volumes ΔV_a from the slopes. As can be seen from Figure 8, the activation volume remains nearly constant at high normal pressures of 3.9–9.8 GPa, which is approximately 1.7 % of the volume of the D-4OH molecules. However, below 3.9 GPa the activation volume increases with decreasing normal pressure. The change of activation volume with pressure is consistent with that observed for solid polymeric material.[68] This result suggests caution in extrapolating the linear stress-activated Arrhenius curve obtained at high normal pressures, which could cause significant overestimation of decomposition rate constants at low normal pressures because the activation volume could be no longer a constant in a wide pressure range.

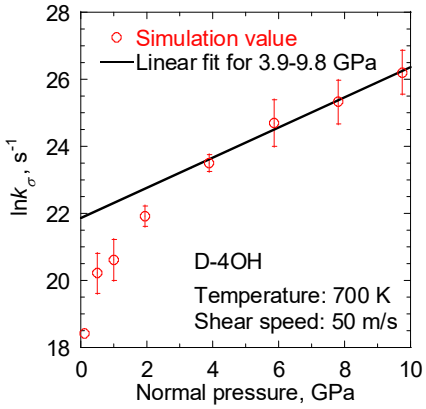

Figure 6. Natural logarithm of stress-dependent decomposition rate constant k_σ for D-4OH as a function of normal pressure. Error bar indicates the standard deviation of 10 independent simulations.

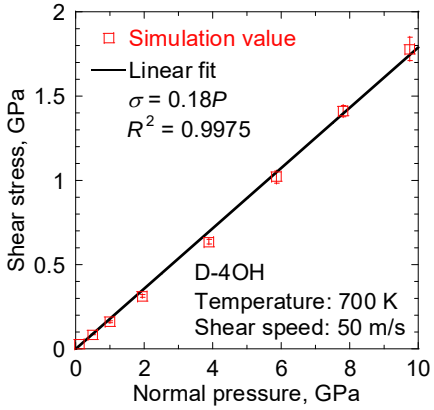

Figure 7. Shear stress versus normal pressures for D-4OH. Error bar indicates the standard deviation of 10 independent simulations.

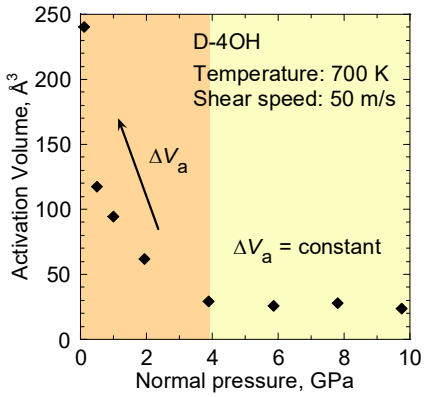

Figure 8. Activation volume as a function of normal pressure for D-4OH.

3.3.2. Effect of Molecular Structure and Mechano-chemical Decomposition Pathways. To investigate the effect of molecular structure on the decomposition rate of PFPE films, we performed shearing simulations for Demnum, Z, D-4OH, and Z-tetraol. To reduce the computational time, a relatively high normal pressure of 7.8 GPa was used. Figure 9 compares the progress of decomposition of the four types of PFPE molecules. The plots of $\ln(N_t/N_0)$ versus time and the linear fits with Eq. (3) are shown in Figure S6 (Supporting Information). We found that polar D-4OH and Z-tetraol decompose more rapidly than nonpolar Demnum and Z, and the nonpolar Z decomposes more rapidly than the nonpolar Demnum.

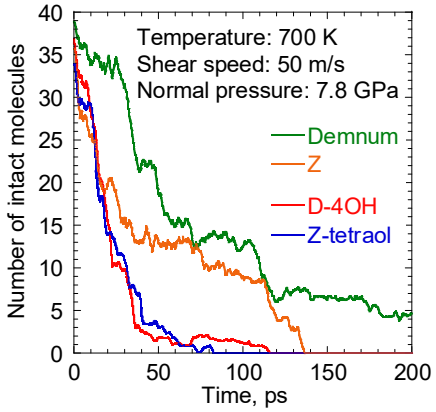

Figure 9. Time evolution of the number of intact PFPE molecules in the 200-ps shearing simulations. Demnum and Z are nonpolar and D-4OH and Z-tetraol are polar molecules.

To understand the underlying mechanism of the above results, we analyzed the decomposition pathways by calculating the dissociation ratios for different types of bonds. Here the dissociation ratio for one type of bond is defined as the ratio of the number of dissociated bonds to the total number of that type of bond. Table 4 lists the analysis results for Z-tetraol, which exhibits the highest decomposition rate as seen from Figure 9. Note that, though data are not shown, similar results were obtained for the other three types of PFPEs. The C–OH and ether C–O bonds in the end groups show the two highest dissociation rates, which are four times larger than the highest

bond dissociation rate in the main chain (i.e., the dissociation rate of the C–O bond in the main chain). This demonstrates that decomposition of PFPE molecules occurs mostly at the polar end groups. This also rationally explain the faster decomposition of polar PFPEs than the nonpolar ones. In the main chain, the C–O bond shows roughly four times larger dissociation rate than the C–C bond. This should be the reason for the faster decomposition of Z than Demnum, as the number of C–O bond in Z is roughly twice that in Demnum.

Table 4. Bond dissociation ratio for Z-tetraol in the shearing simulation.

Bond location	Bond type	Bond dissociation ratio (%)
Main chain	C–C	3.43
	C–O	13.2
	C–F	0.00
End group	C–C	3.43
	C–O (ether bond)	58.8
	C–O (C–OH group)	63.8
	C–H	0.00
	O–H	16.9

4. CONCLUSIONS

We developed a ReaxFF force field for PFPE, and using this force field we performed reactive MD simulations to gain insights into mechano-chemical decomposition of nanometer-thick PFPE films at the HDI of HAMR. For comparison, pure thermal decomposition of bulk PFPE was also

simulated. The logarithm of the rate constant of pure thermal decomposition exhibits a linear relation with the reciprocal of temperature, indicating Arrhenius behavior. The time constant of pure thermal decomposition was estimated from the Arrhenius plot to be 11 and 0.078 s at the HAMR operation temperatures of 700 and 800 K. In contrast, the decomposition time constant decreased to approximately 10 ns when PFPE films were subjected to normal impact or horizontal shear from the head at normal pressure of 0.1 GPa and shear speed of 50 m/s, in addition to heating at 700 K. We thus concluded that, within the 1 ns heating time of HAMR, pure thermal decomposition hardly occurs, whereas mechano-chemical decomposition is highly likely to occur.

Our simulations results showed that the decomposition rate constant of PFPE films subjected to confined shear increases with normal pressure. The increase is well fitted by a linear stress-activated Arrhenius curve at high normal pressures, whereas this is not the case at low normal pressures. According to the stress-assisted reaction rate theory, the deviation at low normal pressures can be interpreted by the change of activation volume. Hence, we caution against extrapolating the linear stress-activated Arrhenius curve obtained at high normal pressures to low normal pressures, which could cause significant overestimation of decomposition rate constants at low normal pressures.

Our simulation results also showed that polar molecules D-4OH and Z-tetraol decompose more rapidly than nonpolar molecules Demnum and Z, and the nonpolar Z decomposes more rapidly than the nonpolar Demnum. We confirmed that the decomposition of PFPE molecules is mainly caused by the dissociation of C–OH and ether C–O bonds in the polar end groups, and in the main chain the C–O bond is more likely to dissociate than the C–C bond. Our findings extend understanding of mechano-chemical decomposition of nanometer-thick liquid films and are instructive for the design of head–disk interface in HAMR.

ASSOCIATED CONTENT

Supporting Information

The Supporting Information is available free of charge.

Procedure for building the corrugated solid surfaces, influence of equilibration of initial configurations with/without the developed ReaxFF, bulk density of D-4OH calculated with the developed ReaxFF, plots of $\ln(N_t/N_0)$ versus time for the impacting and shearing simulations (PDF)

AUTHOR INFORMATION

Corresponding Author

*E-mail: zhang@i.nagoya-u.ac.jp

Present Addresses

†Department of Complex Systems Science, Graduate School of Informatics, Nagoya University, Furo-cho, Chikusa-ku, Nagoya 464-8601, Japan

‡Department of Micro-Nano Systems Engineering, Graduate School of Engineering, Nagoya University, Furo-cho, Chikusa-ku, Nagoya 464-8603, Japan

ACKNOWLEDGMENT

This work was supported in part by the JSPS Grant-in-Aid for Scientific Research (B No. 17H03164), a grant from the Advanced Storage Research Consortium, and Nagoya University High Performance Computing Research Project for Joint Computational Science. Xingyu Chen would like to acknowledge the financial support from China Scholarship Council (CSC) (No. 201907090093).

REFERENCES

(1) Kryder, M. H.; Gage, E. C.; McDaniel, T. W.; Challener, W. A.; Rottmayer, R. E.; Ju, G. Heat Assisted Magnetic Recording. *Proc. IEEE* **2008**, *96*, 1810–1835.

(2) Huang, L.; Stipe, B.; Staffaroni, M.; Juang, J.; Hirano, T.; Schreck, E.; Huang, F. HAMR Thermal Modeling Including Media Hot Spot. *IEEE Trans. Magn.* **2013**, *49*, 2565–2568.

(3) Kiely, J. D.; Jones, P. M.; Hoehn, J. Materials Challenges for the Heat-Assisted Magnetic Recording Head-Disk Interface. *MRS Bull.* **2018**, *43*, 119–124.

(4) Rajauria, S.; Ruiz, O.; Canchi, S. V.; Schreck, E.; Dai, Q. Electrostatically Tunable Adhesion in a High Speed Sliding Interface. *Phys. Rev. Lett.* **2018**, *120*, 026101.

(5) Spikes, H. Stress-Augmented Thermal Activation: Tribology Feels the Force. *Friction* **2018**, *6*, 1–31.

(6) Kiely, J. D.; Jones, P. M.; Yang, Y.; Brand, J. L.; Anaya-Dufresne, M.; Fletcher, P. C.; Zavaliche, F.; Toivola, Y.; Duda, J. C.; Johnson, M. T. Write-Induced Head Contamination in Heat-Assisted Magnetic Recording. *IEEE Trans. Magn.* **2017**, *53*, 1–7.

(7) Fowler, D. E.; Geiss, R. H. Chemical Contamination at the Head-Disk Interface in a Disk Drive. *IEEE Trans. Magn.* **2000**, *36*, 133–139.

(8) Xiong, S.; Wang, N.; Smith, R.; Li, D.; Schreck, E.; Dai, Q. Material Transfer Inside Head Disk Interface for Heat Assisted Magnetic Recording. *Tribol. Lett.* **2017**, *65*, 74.

(9) Ghahri Sarabi, M. S.; Bogy, D. B. Simulation of the Performance of Various PFPE Lubricants Under Heat Assisted Magnetic Recording Conditions. *Tribol. Lett.* **2014**, *56*, 293–304.

(10) Yang, Y.; Li, X.; Stirniman, M.; Yan, X.; Huang, F.; Zavaliche, F.; Wang, H.; Huang, J.; Tang, H.; Jones, P. M.; et al. Head-Disk Lubricant Transfer and Deposition During Heat-Assisted Magnetic Recording Write Operations. *IEEE Trans. Magn.* **2015**, *51*, 1–4.

(11) Ji, R.; Xu, J.; Liew, T.; Zhang, J.; Xie, H. Q.; Xu, B.; Dao, T. K. L. TOF-SIMS Analysis of Media Lubricant under Laser Irradiation for HAMR Application. *Surf. Interface Anal.* **2011**, *43*, 406–409.

(12) Li, L.; Jones, P. M.; Hsia, Y.-T. Effect of Chemical Structure and Molecular Weight on High-Temperature Stability of Some Fomblin Z-Type Lubricants. *Tribol. Lett.* **2004**, *16*, 21–27.

(13) Tani, H.; Shibahara, Y.; Lu, R.; Koganezawa, S.; Tagawa, N. TOF-SIMS Analysis of Perfluoropolyether Lubricant Smear Transferred from Disk Surface Following Laser Heating. *Microsyst. Technol.* **2020**, *26*, 79–88.

(14) Murugesan, V.; Cho, J. S.; Govind, N.; Andersen, A.; Olszta, M. J.; Han, K. S.; Li, G.; Lee, H.; Reed, D. M.; Sprenkle, V. L.; et al. Lithium Insertion Mechanism in Iron Fluoride

Nanoparticles Prepared by Catalytic Decomposition of Fluoropolymer. *ACS Appl. Energy Mater.* **2019**, *2*, 1832–1843.

(15) Lotfi, R.; van Duin, A. C. T.; Biswas, M. M. Molecular Dynamics Simulations of Perfluoropolyether Lubricant Degradation in the Presence of Oxygen, Water, and Oxide Nanoparticles Using a ReaxFF Reactive Force Field. *J. Phys. Chem. C* **2018**, *122*, 2684–2695.

(16) Helmick, L. S.; Jones, W. R. Determination of the Thermal Stability of Perfluoroalkylethers. *National Aeronautics and Space Administration* **1990**, NASA Technical Memorandum-102493.

(17) Zhao, X.; Bhushan, B. Comparison Studies on Degradation Mechanisms of Perfluoropolyether Lubricants and Model Lubricants. *Tribol. Lett.* **2001**, *9*, 187–197.

(18) Tao, Z.; Bhushan, B. Degradation Mechanisms and Environmental Effects on Perfluoropolyether, Self-Assembled Monolayers, and Diamondlike Carbon Films. *Langmuir* **2005**, *21*, 2391–2399.

(19) Tao, Z.; Bhushan, B. Bonding, Degradation, and Environmental Effects on Novel Perfluoropolyether Lubricants. *Wear* **2005**, *259*, 1352–1361.

(20) Tanaka, K.; Kato, T.; Matsumoto, Y. Molecular Dynamics Simulation of Vibrational Friction Force Due to Molecular Deformation in Confined Lubricant Film. *J. Tribol.* **2003**, *125*, 587–591.

(21) Dai, L.; Sorkin, V.; Sha, Z. D.; Pei, Q. X.; Branicio, P. S.; Zhang, Y. W. Molecular Dynamics Simulations on the Frictional Behavior of a Perfluoropolyether Film Sandwiched between Diamond-like-Carbon Coatings. *Langmuir* **2014**, *30*, 1573–1579.

(22) Sorkin, V.; Sha, Z. D.; Branicio, P. S.; Pei, Q. X.; Zhang, Y. W. Atomistic Molecular Dynamics Study of Structural and Thermomechanical Properties of Zdol Lubricants on Hydrogenated Diamond-Like Carbon. *IEEE Trans. Magn.* **2013**, *49*, 5227–5235.

(23) Nath, S. K. D.; Wong, C. H.; Sorkin, V.; Sha, Z. D.; Zhang, Y. W.; Kim, S. G. Study of the Spreading of Perfluoropolyether Lubricants on a Diamond-Like Carbon Film. *Tribol. Trans.* **2013**, *56*, 255–267.

(24) Li, B.; Wong, C. H.; Chen, Q. Kinetics of Lubricant Desorption and Decomposition under Heat Treatment: A Molecular Dynamics Study. *Soft Matter* **2013**, *9*, 700–708.

(25) Deb Nath, S. K. Thermal Decomposition and Desorption of PFPE Zdol on a DLC Substrate Using Quartic Bond Interaction Potential. *RSC Adv.* **2015**, *5*, 69651–69659.

(26) Lotfi, R.; Jonayat, A.; van Duin, A. C. T.; Biswas, M. M.; Hempstead, R. A Reactive Force Field Study on the Interaction of Lubricant with Diamond-Like Carbon Structures. *J. Phys. Chem. C* **2016**, *120*, 27443–27451.

(27) van Duin, A. C. T.; Dasgupta, S.; Lorant, F.; Goddard, W. A. ReaxFF: A Reactive Force Field for Hydrocarbons. *J. Phys. Chem. A* **2001**, *105*, 9396–9409.

(28) Chenoweth, K.; van Duin, A. C. T.; Goddard, W. A. ReaxFF Reactive Force Field for Molecular Dynamics Simulations of Hydrocarbon Oxidation. *J. Phys. Chem. A* **2008**, *112*, 1040–1053.

(29) Ashraf, C.; van Duin, A. C. T. Extension of the ReaxFF Combustion Force Field toward Syngas Combustion and Initial Oxidation Kinetics. *J. Phys. Chem. A* **2017**, *121*, 1051–1068.

(30) Ashraf, C.; Shabnam, S.; Jain, A.; Xuan, Y.; van Duin, A. C. T. Pyrolysis of Binary Fuel Mixtures at Supercritical Conditions: A ReaxFF Molecular Dynamics Study. *Fuel* **2019**, *235*, 194–207.

(31) Senftle, T. P.; Hong, S.; Islam, M. M.; Kylasa, S. B.; Zheng, Y.; Shin, Y. K.; Junkermeier, C.; Engel-Herbert, R.; Janik, M. J.; Aktulga, H. M.; et al. The ReaxFF Reactive Force-Field: Development, Applications and Future Directions. *npj Comput. Mater.* **2016**, *2*, 1–14.

(32) Ewen, J. P.; Latorre, C. A.; Gattinoni, C.; Khajeh, A.; Moore, J. D.; Remias, J. E.; Martini, A.; Dini, D. Substituent Effects on the Thermal Decomposition of Phosphate Esters on Ferrous Surfaces. *J. Phys. Chem. C* **2020**, *124*, 9852–9865.

(33) Plimpton, S. J.; Thompson, A. P. Computational Aspects of Many-Body Potentials. *MRS Bull.* **2012**, *37*, 513–521.

(34) Ashurst, W. T.; Hoover, W. G. Dense-Fluid Shear Viscosity via Nonequilibrium Molecular Dynamics. *Phys. Rev. A* **1975**, *11*, 658–678.

(35) Ewen, J. P.; Heyes, D. M.; Dini, D. Advances in Nonequilibrium Molecular Dynamics Simulations of Lubricants and Additives. *Friction* **2018**, *6*, 349–386.

(36) Martini, A.; Eder, S. J.; Dörr, N. Tribochemistry: A Review of Reactive Molecular Dynamics Simulations. *Lubricants* **2020**, *8*, 44.

(37) Ding, J.; Zhang, L.; Zhang, Y.; Han, K.-L. A Reactive Molecular Dynamics Study of N-Heptane Pyrolysis at High Temperature. *J. Phys. Chem. A* **2013**, *117*, 3266–3278.

(38) Khajeh, A.; He, X.; Yeon, J.; Kim, S. H.; Martini, A. Mechanochemical Association Reaction of Interfacial Molecules Driven by Shear. *Langmuir* **2018**, *34*, 5971–5977.

(39) Jacobs, T. D. B.; Gotsmann, B.; Lantz, M. A.; Carpick, R. W. On the Application of Transition State Theory to Atomic-Scale Wear. *Tribol. Lett.* **2010**, *39*, 257–271.

(40) Gosvami, N. N.; Bares, J. A.; Mangolini, F.; Konicek, A. R.; Yablon, D. G.; Carpick, R. W. Mechanisms of Antiwear Tribofilm Growth Revealed in Situ by Single-Asperity Sliding Contacts. *Science* **2015**, *348*, 102–106.

(41) Jacobs, T. D. B.; Carpick, R. W. Nanoscale Wear as a Stress-Assisted Chemical Reaction. *Nat. Nano.* **2013**, *8*, 108–112.

(42) Vahdat, V.; Ryan, K. E.; Keating, P. L.; Jiang, Y.; Adiga, S. P.; Schall, J. D.; Turner, K. T.; Harrison, J. A.; Carpick, R. W. Atomic-Scale Wear of Amorphous Hydrogenated Carbon during Intermittent Contact: A Combined Study Using Experiment, Simulation, and Theory. *ACS Nano* **2014**, *8*, 7027–7040.

(43) Wang, Y.; Shi, Y.; Sun, Q.; Lu, K.; Kubo, M.; Xu, J. Development of a Transferable ReaxFF Parameter Set for Carbon- and Silicon-Based Solid Systems. *J. Phys. Chem. C* **2020**, *124*, 10007–10015.

(44) Islam, M. M.; Bryantsev, V. S.; van Duin, A. C. T. ReaxFF Reactive Force Field Simulations on the Influence of Teflon on Electrolyte Decomposition during Li/SWCNT Anode Discharge in Lithium-Sulfur Batteries. *J. Electrochem. Soc.* **2014**, *161*, E3009–E3014.

(45) Frisch, M. J.; Trucks, G. W.; Schlegel, H. B.; Scuseria, G. E.; Robb, M. A.; Cheeseman, J. R.; Scalmani, G.; Barone, V.; Petersson, G. A.; Nakatsuji, H.; et al. *Gaussian 16, Revision C.01*; Gaussian, Inc.: Wallingford, CT, 2016.

(46) Becke, A. D. A New Mixing of Hartree-Fock and Local Density-Functional Theories. *J. Chem. Phys.* **1993**, *98*, 1372–1377.

(47) Lee, C.; Yang, W.; Parr, R. G. Development of the Colle-Salvetti Correlation-Energy Formula into a Functional of the Electron Density. *Phys. Rev. B* **1988**, *37*, 785–789.

(48) Hehre, W. J.; Ditchfield, R.; Pople, J. A. Self-Consistent Molecular Orbital Methods. XII. Further Extensions of Gaussian-Type Basis Sets for Use in Molecular Orbital Studies of Organic Molecules. *J. Chem. Phys.* **1972**, *56*, 2257–2261.

(49) Hariharan, P. C.; Pople, J. A. The Influence of Polarization Functions on Molecular Orbital Hydrogenation Energies. *Theor. Chim. Acta* **1973**, *28*, 213–222.

(50) Ditchfield, R.; Hehre, W. J.; Pople, J. A. Self-consistent Molecular-orbital Methods. IX. An Extended Gaussian-type Basis for Molecular-orbital Studies of Organic Molecules. *J. Chem. Phys.* **1971**, *54*, 724–728.

(51) AMS. *SCM, Theoretical Chemistry, Vrije Universiteit, Amsterdam, The Netherlands*.

(52) Sque, S. J.; Jones, R.; Briddon, P. R. Structure, Electronics, and Interaction of Hydrogen and Oxygen on Diamond Surfaces. *Phys. Rev. B* **2006**, *73*, 085313.

(53) Voeltzel, N.; Fillot, N.; Vergne, P.; Joly, L. Orders of Magnitude Changes in the Friction of an Ionic Liquid on Carbonaceous Surfaces. *J. Phys. Chem. C* **2018**, *122*, 2145–2154.

(54) Guo, L.; Chen, S.; Robbins, M. O. Effective Slip Boundary Conditions for Sinusoidally Corrugated Surfaces. *Phys. Rev. Fluids* **2016**, *1*, 074102.

(55) Kobayashi, T.; Zhang, H.; Fukuzawa, K.; Itoh, S. Coarse-Grained Molecular Dynamic Simulations of Nanometer-Thick Polar Lubricant Films Sheared Between Solid Surfaces With Random Roughness. *IEEE Trans. Magn.* **2015**, *51*, 1–4.

(56) Zhang, H.; Fukuda, M.; Washizu, H.; Kinjo, T.; Yoshida, H.; Fukuzawa, K.; Itoh, S. Shear Thinning Behavior of Nanometer-Thick Perfluoropolyether Films Confined between Corrugated Solid Surfaces: A Coarse-Grained Molecular Dynamics Study. *Tribol. Int.* **2016**, *93*, 163–171.

(57) Lu, R.; Zhang, H.; Mitsuya, Y.; Fukuzawa, K.; Itoh, S. Influence of Surface Roughness and Coating on the Friction Properties of Nanometer-Thick Liquid Lubricant Films. *Wear* **2014**, *319*, 56–61.

(58) Sun, H. COMPASS: An Ab Initio Force-Field Optimized for Condensed-Phase Applications-Overview with Details on Alkane and Benzene Compounds. *J. Phys. Chem. B* **1998**, *102*, 7338–7364.

(59) Plimpton, S. Fast Parallel Algorithms for Short-Range Molecular Dynamics. *J. Comput. Phys.* **1995**, *117*, 1–19.

(60) Nosé, S. A Molecular Dynamics Method for Simulations in the Canonical Ensemble. *Mol. Phys.* **1984**, *52*, 255–268.

(61) Hoover, W. G. Canonical Dynamics: Equilibrium Phase-Space Distributions. *Phys. Rev. A* **1985**, *31*, 1695–1697.

(62) Bernardi, S.; Todd, B. D.; Searles, D. J. Thermostating Highly Confined Fluids. *J. Chem. Phys.* **2010**, *132*, 244706.

(63) Guan, Y.; Lou, J.; Liu, R.; Ma, H.; Song, J. Reactive Molecular Dynamics Simulation on Thermal Decomposition of N-Heptane and Methylcyclohexane Initiated by Nitroethane. *Fuel* **2020**, *261*, 116447.

(64) Arrhenius, S. Über Die Reaktionsgeschwindigkeit Bei Der Inversion von Rohrzucker Durch Säuren. *Z. Phys. Chem.* **1889**, *4*, 226–248.

(65) Zhang, J.; Spikes, H. On the Mechanism of ZDDP Antiwear Film Formation. *Tribol. Lett.* **2016**, *63*, 24.

(66) Zhang, J.; Ewen, J. P.; Ueda, M.; Wong, J. S. S.; Spikes, H. A. Mechanochemistry of Zinc Dialkyldithiophosphate on Steel Surfaces under Elastohydrodynamic Lubrication Conditions. *ACS Appl. Mater. Interfaces* **2020**, *12*, 6662–6676.

(67) Yeon, J.; He, X.; Martini, A.; Kim, S. H. Mechanochemistry at Solid Surfaces: Polymerization of Adsorbed Molecules by Mechanical Shear at Tribological Interfaces. *ACS Appl. Mater. Interfaces* **2017**, *9*, 3142–3148.

(68) Nobrega, M. M.; Ceppatelli, M.; Temperini, M. L. A.; Bini, R. Pressure-Induced Reactivity in the Emeraldine Salt and Base Forms of Polyaniline Probed by FTIR and Raman. *J. Phys. Chem. C* **2014**, *118*, 27559–27566.

TOC Graphic

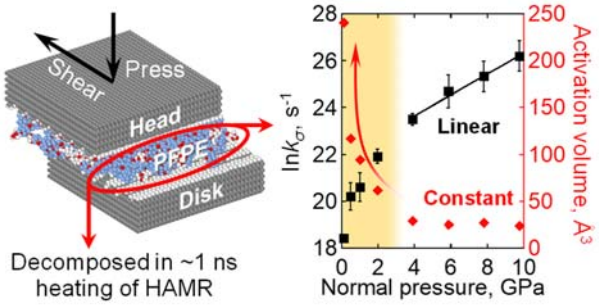
Shear
Press
Head
PFPE
Disk
Decomposed in ~1 ns
heating of HAMR
28
26
24
22
20
18
lnk$_\sigma$, s^{-1}
250
200
150
100
50
0
Activation volume, Å^3
Linear
Constant
0
2
4
6
8
10
Normal pressure, GPa